Temperature-induced effect on refractive index of graphene based on coated in-fiber Mach–Zehnder interferometer*

Li-Jun Li(李丽君)[1,2,3,†], Shun-Shun Gong(宫顺顺)[1], Yi-Lin Liu(刘仪琳)[1], Lin Xu(徐琳)[1], Wen-Xian Li(李文宪)[1], Qian Ma(马茜)[3], Xiao-Zhe Ding(丁小哲)[1], and Xiao-Li Guo(郭晓丽)[1]

[1] College of Electronics, Communication and Physics, Shandong University of Science and Technology, Qingdao 266590, China

[2] State Key Laboratory of Mining Disaster Prevention and Control Co-founded by Shandong Province and the Ministry of Science and Technology, Shandong University of Science and Technology, Qingdao 266590, China

[3] College of Electrical Engineering and Automation, Shandong University of Science and Technology, Qingdao 266590, China

(Received 26 June 2017; revised manuscript received 27 July 2017; published online 30 September 2017)

The temperature-induced complex refractive index (CRI) effect of graphene is demonstrated theoretically and experimentally based on a graphene coated in-fiber MZI (Mach–Zehnder interferometer). The relationships between real and imaginary parts of the graphene CRI and temperature are obtained through investigating the dip wavelength and intensity of the MZI interference spectrum changing with temperature, respectively. The temperature effect of CRI of the graphene is also analyzed theoretically. Both experimental and theoretical studies show that the real part and imaginary part of the CRI nonlinearly decrease and increase with temperature increasing, respectively. This graphene-coated in-fiber MZI structure also possesses the advantages of easy fabrication, miniaturization, low cost and robustness. It has potential applications in nanomaterial-based optic devices for communication and sensing.

Keywords: in-fiber Mach–Zehnder interferometer, graphene, temperature-induced, complex refractive index

PACS: 65.80.Ck, 68.65.Pq, 78.67.Wj, 42.81.–i **DOI:** 10.1088/1674-1056/26/11/116504

1. Introduction

Graphene is a honeycomb-shaped sheet of carbon atoms arranged. It is one-atom thick ($\sim$ 0.34 nm) and has attractive properties, such as good transparency,[1,2] medium notable nonlinearity,[3] broadband polarization,[4,5] and strong conductivity.[6] Its conductivity closely relates to the electromagnetic wave frequency, surrounding temperature and the Fermi level of the dopant, which makes graphene have great potential applications in nano integrated devices of communications and sensing.[7–10] All optical fiber sensors have received great research interest and have been wildly applied to biological, chemical, and environmental industries, due to their unique advantages of high sensitivity, compact size, low cost, and immunity to electromagnetic interference, and so on.[11,12] So far, there are some demonstrations of the combination of graphene and varieties of optical fiber sensing structures, such as titled optical fiber grating,[13] etched fiber Bragg grating,[14] and microfibers.[15] By using various optical properties of graphene, some graphene coated devices are obtained. Because of the interactions between the excited backward propagating cladding modes of the tilted optical fiber grating and the grapheme film, some humidity and refractive index sensors are proposed.[16–18] Optical biosensing and gas-sensing devices based on the etched fiber Bragg gratings coated with graphene with high sensing sensitivity, relative low attenuation, and large dynamic range are demonstrated.[18,19] Microscalegraphene-coated microfibers or side polished fiber as saturable absorbers, light controller, wavelength converter, and sensors are studied.[19–23] Compared with optical fiber Bragg gratings, in-fiber Mach–Zehnder and Michelson interferometer sensors have their own unique advantages such as high sensitivity, low cost, easy fabrication, etc. In 2016, the complex refractive index (CRI) of the graphene was demonstrated by detecting the phase and intensity variation of the Raman spectrum of a two-arm Mach–Zehnder interferometer, in which the sensing arm is attached to a graphene substrate.[24] In 2016, a temperature induced refractive index (RI) influence of graphene-assisted microfiber temperature sensor from 30 °C to 80 °C was demonstrated by detecting the optical power of the Raman spectrum varying with temperature.[7] However, microfibers are often used in these reports, which are drawn from the $\sim$ 1-μm-diameter and $\sim$ 2-mm-long single-mode optical fiber (SMF) with poor robustness sensing structure and complex fabrication process. In addition, the Raman spectrum of the microfiber is not at the conventional communication wavelength, which makes it an inconvenience to the application of conventional optical fiber active and passive devices in these devices, thereby increasing the cost of the systems.

*Project supported by the Shandong Provincial Natural Science Foundation of China (Grant Nos. ZR2009AM017 and ZR2013FM019), the National Postdoctoral Project of China (Grant Nos. 200902574 and 20080441150), the Shandong Provincial Education Department Foundation of China (Grant No. J06P14), and the Opening Foundation of State Key Lab of Minning Disaster Prevention and Control Co-founded by Shandong Province and the Ministry of Science and Technology of China (Grant No. MDPC201602).

†Corresponding author. E-mail: nankaillj@163.com

© 2017 Chinese Physical Society and IOP Publishing Ltd

In this paper, the effect of temperature on the refractive index of graphene based on a graphene coated in-fiber Mach–Zehnder interferometer (MZI) is demonstrated. In this study, grapheneis coated on the cladding that is partly etched by MTM (single mode-multimode-thined core-multimode-single mode) in-fiber MZI, through the direct deposition method. The temperature-induced effect of the refractive index of graphene is demonstrated through comparing the interference spectra between graphene coated MZI and uncoated MZI indifferent ambient temperatures in a range from 40 °C to 300 °C. It is found that the temperature can cause the CRI of the graphene to change. This temperature effect makes the real and imaginary parts of the CRI of the graphene change with the temperature. By measuring the variation of the interference spectrum of MZI, the relationships between the real and imaginary parts and temperature are obtained. This effect is also theoretically analyzed, which shows that the simulation and experimental results agree with each other. These results are also adoptable in the other CRIs of carbon nanomaterials such as carbon nanotubes and fullerenes. Meanwhile, this graphene-coated in-fiber MZI structure also presents special superiorities including easy fabrication, miniaturization, low cost, and robustness.

2. Experimental setup and graphene coating process

2.1. Experimental setup

The configuration of the graphene-coated in-fiber MZI is shown in Fig. 1. This structure consists of a section of etched-cladding thined core fiber (TCF) spliced between two short sections of multimode fibers (MMFs). The TCF is 15 mm long with a 4.5/125 μm core/cladding diameter ratio. Two sections of MMFs are spliced with the two ends of the TCF. Each of the two MMF sections is 5 mm long, and has a 105/125 μm core/cladding diameter ratio and 0.22 NA (Numerical Aperture), and pure silica core, specifically, multimode optical fiber produced by the Nufern company. Two sections of Corning standard SMFs are spliced at the two ends of the MTM as input and output optical fiber function, respectively.

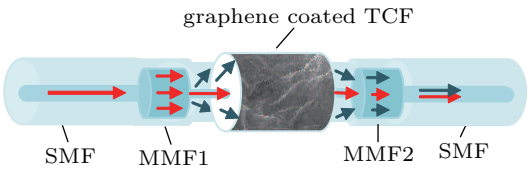


Fig. 1. (color online) Schematic diagram of in-fiber MZI coated with graphene.

The experimental setup is shown in Fig. 2. It include a BBS (broad band light source) with a wavelength range from 1531 nm to 1565 nm, an adjustable temperature box with 0.1 °C resolution and an OSA (optical spectrum analyzer). The graphene coated MZI section is placed in the temperature box.

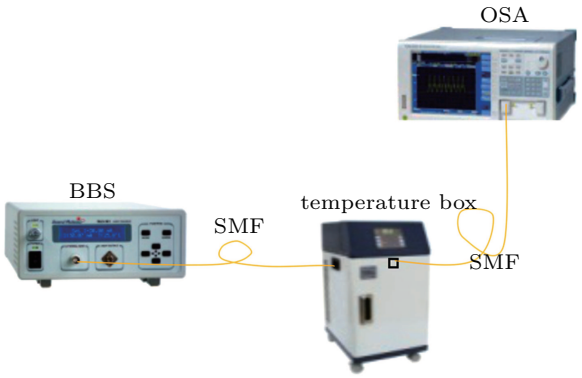


Fig. 2. (color online) Experimental setup.

2.2. Graphene coating process

The MZI structure is shown in Fig. 1. Before it is coated, the thined-core fiber is etched by utilizing hydrofluoric acid. Then, the etched TCF is washed with deionized water several times until its spectrum is no longer changed, which means that the hydrofluoric acid is cleansed. After that, the TCF is placed into NaOH solution for minutes at room temperature, which can not only neutralize the residual H^+, but also make the fiber surface hydrophilic by creating a few OH- groups on the surface of the TCF. The graphene is ultrasonically dispersed in pure dimethylfomamide (DMF) solution for several hours to prepare the graphene coating solution. The etched TCF is placed in a V-type groove and the graphene coating solution is deposited on the surface of the TCF while it is kept in a constant temperature box. After the graphene attaches tightly to the surface of the fiber, the graphene coating film on the fiber is achieved. In order to obtain the required thickness, the coating process can be repeated several times. In our experiments, the graphene is the single-layered graphene with higher than 99% purity, 0.6-to-1 nm thickness, 0.5-to-5 μm slice diameter, and 1000-to-1217 m^2/g specific surface area. Figure 3 shows the scanning electron micrograph (SEM) of the graphene coated MZI. Figure 3(a) shows the SEM image of graphene coating MMF. It can be found that the graphene is deposited around the cylindrical surface along its radial direction with 127.3 μm diameter. So we can estimate the thickness of this graphene film to be about 2.3 μm. Figure 3(b) is the SEM image of the graphene coated on the etched TCF with 103.5 μm diameter, which means that the TCF cladding is etched to a depth of about 20–25 μm. Figure 3(c) is a high-resolution image of the graphene coating, in which lamellar graphene structures covering the surface of the fiber can be observed. Figure 3(d) is the high-resolution image of the graphene coating surface. From this figure, it can be found that a close graphene coating is formed on the fiber surface.

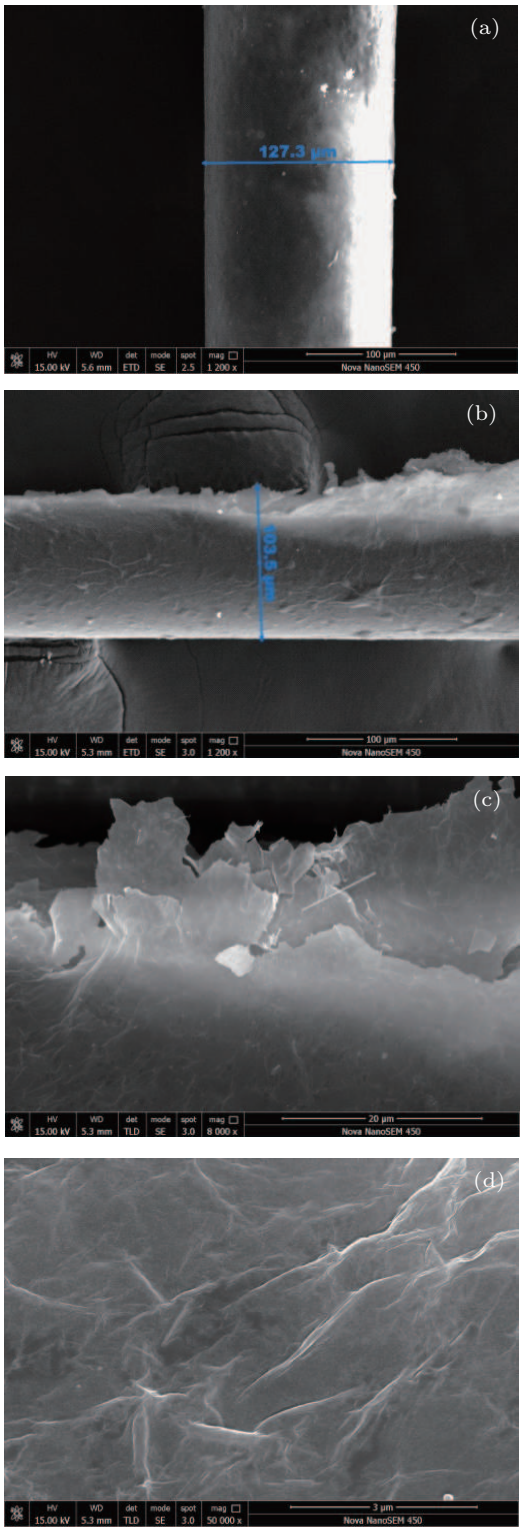


Fig. 3. (a) SEM image of the graphene coated around the circular surface of optical fiber. (b) SEM image of graphene coated around the surface of etched TCF. (c) High-resolution image of lamellar structures of the graphene coating. (d) High-resolution image of the graphene coating surface on the fiber.

3. Graphene temperature-induced RI effect

3.1. Temperature characteristics of uncoated in-fiber MZI

As a basic characteristic, the temperature of uncoated in-fiber MZI is first characterized in the heating procedure from 40 °C to 300 °C. Figure 4(a) shows the interference spectrum versus temperature. From this figure, it can be found that the dipwavelength has a red-shift and the intensity increases with temperature increasing. Figures 4(b) and 4(c) show the experimental results of dip wavelength and its intensity versus temperature, respectively. Its linearly fitting curve shows that while the temperature rises, the dip wavelength is linearly red-shifted with a sensitivity of 70 pm/°C and 99.91% linearity fitting degree, its intensity gradually increases with a rate of 0.044 dB/°C.

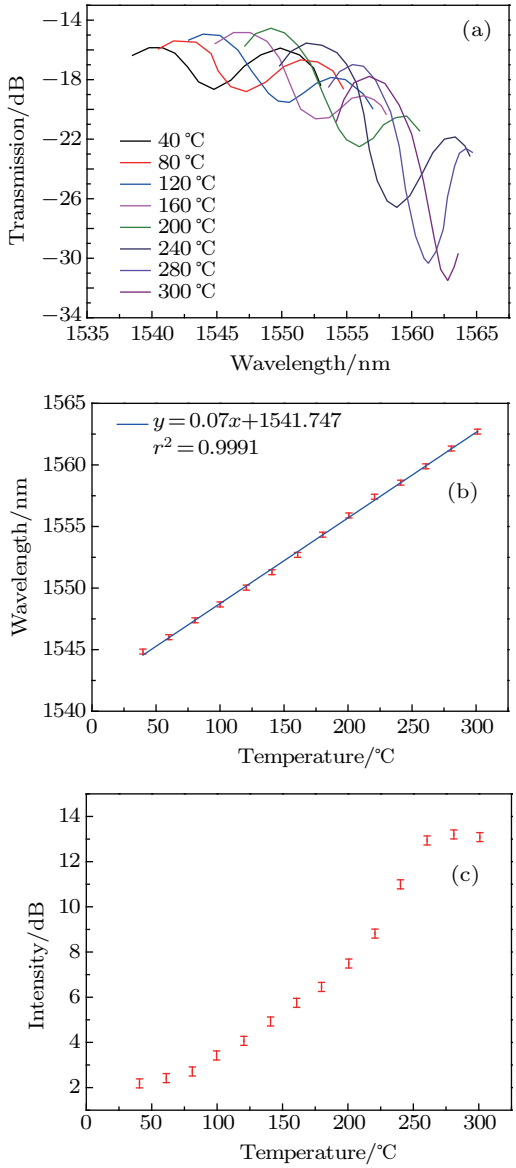


Fig. 4. (color online) (a) Transmission interference spectrum versus temperature of uncoated MZI, (b) linear fits of dip wavelength, and (c) intensity versus temperature of sensor.

3.2. Graphene temperature-induced effect

The graphene temperature-induced RI effect is investigated through studying the relationship between the transmission interference spectrum of graphene coated in-fiber MZI and its surrounding temperature. Figure 5(a) shows the dip wavelength changes with temperature from 40 to 300 °C of the graphene coating MZI. It can be found that the dip wave-

length has a red-shift and its intensity decreases with the surrounding temperature increasing. Figures 5(b) and 5(c) are dip wavelength and intensity versus surrounding temperature and their quadratic fitting curves, respectively. The dip wavelength presents a nonlinear red-shift with the surrounding temperature increasing with a 99.95% quadratic fitting degree. The intensity nonlinearly decreases with increasing temperature.

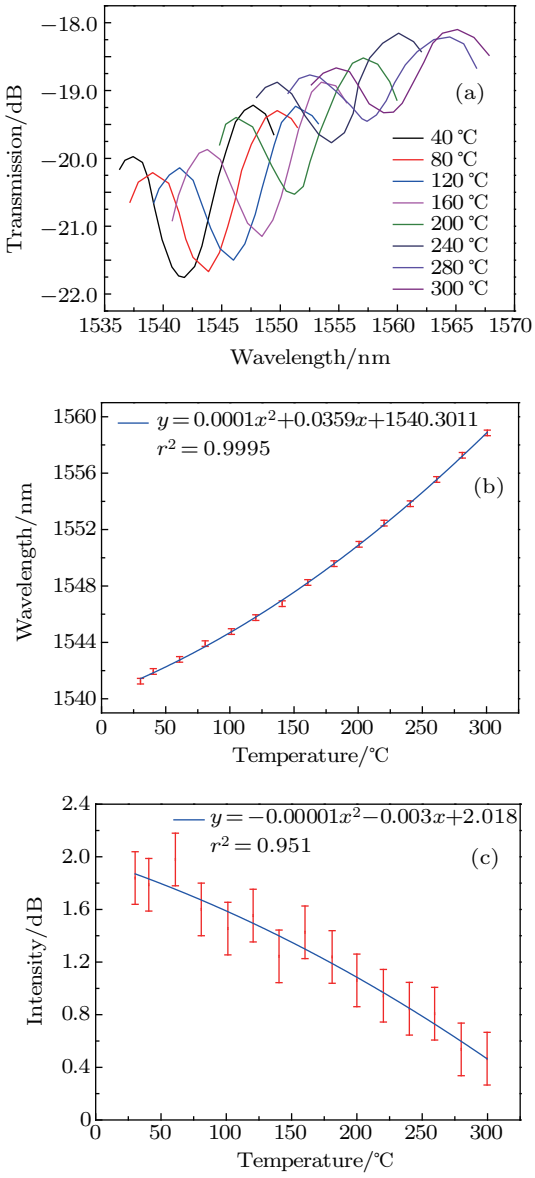


Fig. 5. (color online) (a) Transmission spectrum and (b) nonlinear fitting of dip wavelength and (c) intensity versus temperature in a range from 40 °C to 300 °C for the graphene coating MZI.

These experimental results show obvious differences in spectrum and temperature characteristic between the coated and uncoated MZI due to the temperature-induced CRI effect of the graphene.

4. Theoretical analyses

As shown in Fig. 1, when the light is injected into the MZI from the input SMF to MMF1, multiple modes will be excited and propagate within it. The light of these multiple modes is coupled from the MMF1 into the TCF, part of the multimodes light enters into the TCF cladding while the rest is coupled into the TCF core. In order to increase the interaction area between the cladding modes and the graphene coating, the cladding of the TCF is etched. Similarly, at the splice point between TCF and MMF2, part of cladding modes of the graphene coating TCF are again coupled into the MMF2, multiple modes of MMF2 are consequently coupled into the lead-out SMF, these cladding and core modes will interfere in the core of the lead-out SMF. This structure can be considered as an in-fiber Mach–Zehnder interferometer and its transmission spectrum can be expressed as[8,16]

$$I(\lambda) = I_{\text{core}} + I_{\text{clad}} + 2\sqrt{I_{\text{core}} I_{\text{clad}}} \times \cos\left[\frac{2\pi(n_{\text{eff,co}} - n_{\text{eff,cl}})\text{L}}{\lambda}\right], \quad (1)$$

where I_{core} and I_{clad} are the light intensities of the core mode and the cladding modes in the core of the lead-out SMF, respectively; $n_{\text{eff,co}}$ and $n_{\text{eff,cl}}$ are the effective refractive indices of the core and cladding modes, respectively; L is geometry length of the TCF; λ is the wavelength of the propagating light.

From Eq. (1), when the interference transmission spectrum intensity reaches its minimum, the wavelength of the m-th order dip wavelength can be written as

$$\lambda_m = \frac{2(n_{\text{eff,co}} - n_{\text{eff,cl}})L}{2m+1}. \quad (2)$$

The sensing section in this MZI structure is graphene coating TCF, and its sensing mechanism is analyzed in theory as follows: the electron-hole concentration of the graphene will increase with its surrounding temperature rising due to thermal excitation, resulting in the rising of the conductivity. The optical conductivity of graphene can be written as[8,24]

$$\sigma = \sigma_{\text{intra}} + \sigma_{\text{inter}}, \quad (3)$$

where σ_{intra} and σ_{inter} are the intra-band electron-photon scattering and the direct inter-band electron transition conductivity of the graphene, respectively. These two conductivities can be evaluated from

$$\sigma_{\text{intra}} = \text{i}\frac{e^2 K_{\text{B}} T}{\pi\hbar(\omega + \text{i}\tau^{-1})} \times \left[\frac{\mu_{\text{c}}}{K_{\text{B}}T} + 2\ln\left(\exp\left(-\frac{\mu_{\text{c}}}{K_{\text{B}}T}\right) + 1\right)\right], \quad (4)$$

$$\sigma_{\text{inter}} = \text{i}\frac{e^2}{4\pi\hbar}\ln\left[\frac{2|\mu_{\text{c}}| - \hbar(\omega + \text{i}\tau^{-1})}{2|\mu_{\text{c}}| + \hbar(\omega + \text{i}\tau^{-1})}\right], \quad (5)$$

where e is the electron charge, $K_{\text{B}} = 1.38065 \times 10^{-23}$ J/K is the Boltzmann constant, T is the temperature, $\hbar = 1.0546 \times 10^{-34}$ J·s is the reduced Plank constant, ω is the radiation frequency, $\tau = \mu_{\text{c}} m_{\text{u}} / e v_{\text{F}}^2$ is the momentum relaxation time,

with $v_F \approx 10^8$ being the Fermi velocity, $m_u \approx 10^4$ cm^2/V·s the impurity-limited direct current mobility, and $\mu_c = 0.2403 \times 10^{-19}$ the chemical potential.

Consequently, the complex conductivity of graphene is

$$\sigma = \sigma_r + i\sigma_i, \tag{6}$$

where σ_r and σ_i are the real part and imaginary part of the conductivity of the graphene. They can be calculated from

$$\sigma_r = \frac{\tau^{-1}}{\omega^2+\tau^{-2}}\left[\frac{e^2\mu_c}{\pi\hbar^2} + \frac{2e^2K_BT}{\pi\hbar^2}\ln\left(\exp\left(-\frac{\mu_c}{K_BT}\right)+1\right)\right], \tag{7}$$

$$\sigma_i = \frac{\omega}{\omega^2+\tau^{-2}}\left[\frac{e^2\mu_c}{\pi\hbar^2} + \frac{2e^2K_BT}{\pi\hbar^2}\ln\left(\exp\left(-\frac{\mu_c}{K_BT}\right)+1\right)\right] + \frac{e^2}{4\pi\hbar}\ln\left[\frac{2|\mu_c| - \hbar(\omega+i\tau^{-1})}{2|\mu_c| + \hbar(\omega+i\tau^{-1})}\right]. \tag{8}$$

From Eqs. (7) and (8), we can see that the real part and imaginary part of the conductivity of the graphene relate to temperature, the modeling results are shown in Figs. 6(a) and 6(b) with temperature T ranging from 0 to 300 °C. From Fig. 6, it can be found that the real part and imaginary part of the conductivity of graphene both nonlinearly increase with rising temperature.

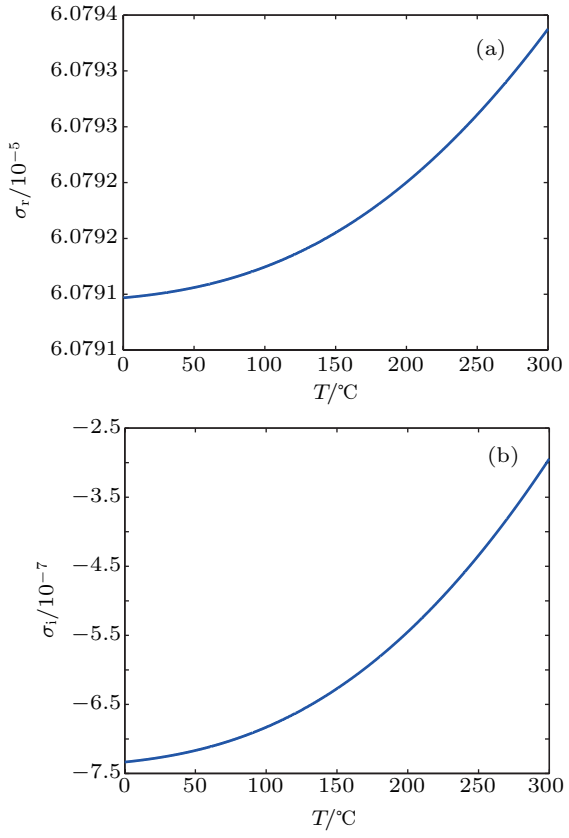


Fig. 6. (color online) Plots of (a) σ_r and (b) σ_i versus temperature in a range from 0 °C to 300 °C.

With the relationship between the conductivity and the complex effective electrical permittivity, the complex electrical permittivity can be expressed as[8,24]

$$\varepsilon_{eff} = 1 + i\sigma/\omega\varepsilon_0 d, \tag{9}$$

where $\varepsilon_0 = 8.85 \times 10^{-12}$ F/m is the vacuum dielectric constant, and d is the thickness of the graphene film on the TCF. The effective refractive index of the graphene can be written as

$$n_{eff} = \sqrt{\varepsilon_{eff}}. \tag{10}$$

The complex refractive index of graphene also has its real part and imaginary part, which can be calculated from

$$n_{gr} = \sqrt{\frac{\sqrt{(\sigma_i - \omega\varepsilon_0 d)^2 + \sigma_r^2} - (\sigma_i - \omega\varepsilon_0 d)}{2\omega\varepsilon_0 d}}, \tag{11}$$

$$n_{gi} = \sqrt{\frac{\sqrt{(\sigma_i - \omega\varepsilon_0 d)^2 + \sigma_r^2} + (\sigma_i - \omega\varepsilon_0 d)}{2\omega\varepsilon_0 d}}, \tag{12}$$

where n_{gr} and n_{gi} are the real and imaginary part of RI of graphene.

Figure 7 shows the simulations of n_{gr} and n_{gi} changing with temperature in a range from 0 °C to 300 °C. From the simulation results, we can see that the real part of CRI nonlinearly decreases and the imaginary part of CRI nonlinearly increases with rising temperature.

Let $n_{eff} = n_{gr} + in_{gi}$, then the transmitting wave in the graphene will be able to be written as

$$E = E_0 e_n \exp[\omega(-n_{gi}r/c)]\exp[i\omega(n_{gr}r/c + t) + \phi_0], \tag{13}$$

where E_0 is the initial amplitude of electric field amplitude, e_n is the unit vector in the direction of electric field vibration, r is the spatial coordinate position along the wave propagation direction, c is the speed of light in a vacuum, t is the time, and ϕ_0 is the initial phase of the light wave. In this equation, for transmitting wave, the $\exp[\omega(-n_{gi}\cdot r/c)]$ part is the attenuation coefficient, and the $\exp[i\omega(n_{gi}\cdot r/c + t) + \phi_0]$ part is the phase change of the interference spectrum.

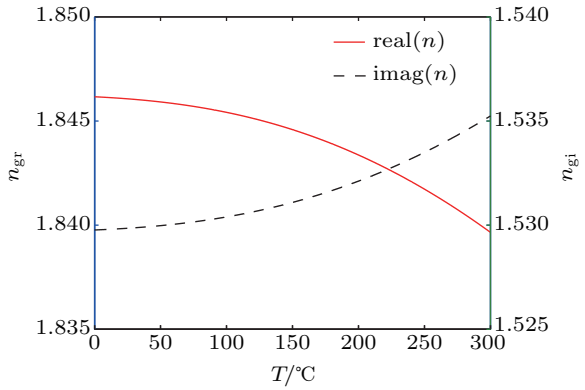


Fig. 7. (color online) Plots of n_{gr} and n_{gi} versus temperature.

Combining Eqs. (1) and (2), we can obtain conclusions that the intensity and the dip wavelength of the transmission interference spectrum of graphene-coating in-fiber MZI will be modulated by changing the complex RI of the graphene.

5. Conclusions and perspective

For the uncoated MZI, as shown in Fig. 4, the dip wavelength and intensity change with temperature, which can be explained as follows: when the surrounding temperature around the TCF increases, both the effective RI of the core and cladding modes increase. Due to the fact that the thermos-optic coefficient of the Ge-doped silica core is higher than that of the cladding consisting of fused silica. From Eq. (2), we can find that the effective RI difference between the core mode and the cladding modes become large with temperature increasing, which will make the dip wavelength of the interference spectrum of the uncoated MZI red-shifted. From Eq. (1), the relationship between the intensity of the uncoated MZI interference spectrum and the temperature can also be explained.

For the graphene coated MZI, the experimental results show that there are temperature characteristics obviously different from those for the uncoated MZI. From Figs. 5(a)–5(c), it can be found that the sensor interference dip wavelength presents a nonlinear red-shift with temperature increasing from 40 °C to 300 °C. The intensity of interference dip wavelength nonlinearly decreases with rising temperature. These can be explained as follows: the effective RI of cladding ($n_{\mathrm{eff,cl}}$) of the graphene coated MZI in Eq. (2) can be seen as the effective RI of the graphene. From Eq. (13), it can be known that the real part (n_{gr}) of the graphene CRI relates to the phase of the interference spectrum of the graphene coated MZI, and from the simulation results of Fig. 7, the temperature increase can cause the real part (n_{gr}) to nonlinearly decrease. As a result of these temperature effects, the effective RI difference between core mode and cladding modes nonlinearly increase with rising temperature, as shown in Fig. 5(b). The relationship between interference spectrum intensity and temperature can be obtained from Eq. (1). For graphene coated MZI, the spectral intensity relates to the imaginary part (n_{gi}) of the graphene CRI as indicated in the $\exp[\omega(-n_{\mathrm{gi}}r/c)]$ equation. From Eq. (1), we can find that the intensity will nonlinearly decrease with increasing temperature as shown in Fig. 5(c). We can obtain a very good quadratic fitting curve between dip wavelength and temperature with a 99.95% fitting degree. From this quadratic fitting cure function, the temperature-induced imaginary part for a transmitting wavelength range from 1531 nm to 1565 nm can be calculated. From the quadratic fitting curve functions of intensity and temperature and considering the imaginary part, the real part can also be calculated.

In conclusion, the temperature-induced CRI effect of graphene is demonstrated theoretically and experimentally through investigating the interference spectrum dip wavelength and intensity of a graphene coated in-fiber MZI changing with its surrounding temperature in a range from 40 to 300 °C. From our simulation results, it can be found that the complex conductivity of graphene can be expressed by a nonlinear relationship between the real and imaginary components of graphene conductivity and the temperature. On this basis, the relationship between the complex RI of the graphene and the temperature is also simulated, and the obtained results show that the real part of the graphene CRI nonlinearly increases and its imaginary part nonlinearly decreases with temperature increasing. In our experiments, a nearly 2-μm-thick graphene film is deposited on the surface of the cladding etched TCF of an in-fiber MZI. Its SEM images show that this film tightly adheres to the optical fiber. Experimental results show that the temperature-induced real part of the CRI of graphene relates to the attenuation coefficient, which causes the intensity to nonlinearly decrease with temperature rising, and the temperature-induced imaginary part of the CRI of graphene relates to the phase change, which causes the dip wavelength to nonlinearly change with temperature. This method can be used not only to detect the temperature-induced CRI of graphene, but also to design graphene-based optic devices for communication and sensing applications.

Acknowledgment

The authors thank Dr. Hui-Ling Zhu of College of Materials Science and Engineering, Shandong University of Science and Technology, China, for providing us with the graphene coating films for SEM measurement.

References

[1] Zhou J T, Wang Y P, Liao C R, Sun B, Jun He, Yin G L, Liu S, Li Z Y, Wang G J, Zhong X Y and Zhao J 2015 *Sens. Act. B: Chem.* **208** 315
[2] Zhang X, Shao J X, Ba D D, Feng Z Z, Chen Y F, Shao J Y and Chen X M 2017 *Acta Phys. Sin.* **66** 026103 (in Chinese)
[3] Nath P, Singh H K, Datta P and Sarma K C 2008 *Sens. Act. A: Phys.* **148** 16
[4] Bhatia V and Vengsarkar A M 1996 *Opt. Lett.* **21** 692
[5] Luo F, Zhu L Q and Meng K 2017 *Chin. Phys. B* **26** 014205
[6] Kang W, Du Y S and Zheng R L 2017 *Acta Phys. Sin.* **66** 014701 (in Chinese)
[7] Li W, Chen B G, Meng C, Fang W, Xiao Y, Li X Y, Hu Z F, Xu Y X, Tong L M, Wang H Q, Liu W T, Bao J M and Shen Y R 2014 *Nano Lett.* **7** 955
[8] Kin F M, Matthew Sfeir Y, Wu Y, Liu C H, James A and Misewich T F 2008 *Phys. Rev. Lett.* **101** 196405
[9] Song C, Xia X S, Hu Z D, Liang Y J and Wang J C 2016 *Nanoscale Res. Lett.* **11** 419
[10] Wang X S, C C, Pan L and Wang J C 2016 *Sci. Rep.* **6** 32616
[11] Erdogan T 1997 *J. Opt. Soc. A* **14** 1760
[12] Li L J, Ma Q, Cao M Y, Zhang G N, Zhang Y, Jiang L, Gao C T, Yao J, Gong S S and Li W X 2016 *Sens. Act. B: Chem.* **234** 674
[13] Jiang B Q, Lu X, Gan X T, Qi M, Wang Y D, Han L, Mao D, Zhang W D, Ren Z Y and Zhao J L 2016 *Opt. Lett.* **40** 3994
[14] Vasu S S, Asokan S and Sood A K 2016 *Opt. Lett.* **41** 2604
[15] Rao Y J, Deng M, Duan D W and Zhu T 2008 *Sens. Act. A: Phys.* **148** 33
[16] Su J, Tong Z R, Cao Y and Zhang W H 2014 *Opt. Commun.* **315** 112
[17] Li L C, Li X, Xie Z H and Liu D M 2012 *Opt. Express* **20** 11109
[18] Harri J, Lu P, Larocque H, Chen L and Bao X 2015 *Sens. Act. B: Chem.* **206** 246
[19] Wang X, Chen Y P and Nolte D D 2008 *Opt. Express* **16** 22105
[20] Sosan C, Kenneth D K, Hong G K, Gyumin L, Jae S P and Joon S L 2014 *Rep* **4** 1
[21] Ju L, Geng B S, Jason H, Caglar G, Michael M, Hao Z, Hans A B, Liang X G, Alex Z Y, Shen R and Wang F 2011 *Nat. Nanotech.* **1** 630
[22] Xu F, Das S, Gong Y, Liu Q, Chien H C, Chiu H Y, Wu J and Hui R 2015 *Appl. Phys. Lett.* **106** 031109
[23] Yao B C, Wu Y, Wang Z G, Cheng Y, Rao Y J, Gong Y, Chen Y F and Li Y R 2013 *Opt. Express* **25** 29818
[24] Sun Q Z, Sun X H, Jia W H, Xu Z L, Luo H P, Liu D M and Zhang L 2016 *Photon. Tech. Lett.* **28** 383